Characterization of a Handheld Gamma Camera for Intraoperative Use for Sentinel Lymph Node Biopsy

Andrew L. Goertzen, *Member, IEEE*, Jonathan D. Thiessen, *Member, IEEE*, Bryan McIntosh, *Student Member, IEEE*, Michael J. Simpson, and James Schellenberg

***Abstract*– Gamma counting probes play an important role in radioguided sentinel lymph node biopsy surgical procedures. The miniaturization of gamma camera components and associated electronics has allowed the introduction of small handheld gamma cameras to be used in place of simple gamma counting probes in these procedures. We report here on the design of a compact handheld gamma camera and first results from the characterization of this device. A handheld gamma camera with field of view 13.2×13.2 mm^2 was constructed based on the SensL SPMArray4SL 4×4 pixel SiPM detector coupled to a 4×4 element CsI:Tl scintillator array with crystal size 3.3×3.3×5 mm^3. The detector is mounted in a 114×32×26 mm^3 ABS plastic enclosure together with a low energy high resolution (LEHR) parallel hole collimator and front end electronics. The total package has a weight of only 320 g. Each SiPM pixel is individually read out using a 2 channel ADC and a custom 8:1 analog multiplexor. The camera is controlled through a custom GUI program written in National Instruments LabView. A preliminary characterization of the detector was performed using a ^{57}Co point source (1 mm diameter). The spatial resolution, measured as the full-width at half-maximum (FWHM) of the crystal response profiles measured by stepping the point source across the detector face in 0.25 mm increments, was 3.46, 3.92, 4.56 and 6.24 mm for source-detector distances of 1, 10, 25 and 50 mm, respectively. The FWHM energy resolution at 122 keV was 40.2% and the detection efficiency was 162.9 and 149.7 cps/MBq for source-detector distances of 1 and 50 mm, respectively. The system count rate vs. incident gamma-ray fluence was linear up to 10^4 cps.**

I. Introduction

GAMMA counting probes have long played an important role in radioguided surgical procedures such as sentinel lymph node biopsy [1, 2]. The miniaturization of gamma camera components and associated electronics has allowed the introduction of small handheld gamma cameras to be used in place of simple gamma counting probes in these procedures [3-7]. To be useful as an intraoperative imaging device, a gamma camera must strike a balance between having a useful field of view (FOV) and being compact, lightweight and ergonomic for use as a handheld device during surgery. In this work we report on the design of a compact handheld gamma camera and the first results from the characterization of this device.

Manuscript received November 22, 2013. This work was supported by an unrestricted research grant from Cubresa, Inc. to A.L. Goertzen.

A.L. Goertzen is with the Department of Radiology and the Department of Physics & Astronomy, University of Manitoba, Winnipeg, Manitoba, Canada. (e-mail: Andrew.Goertzen@med.umanitoba.ca)

J.D. Thiessen is with the Department of Radiology, University of Manitoba, Winnipeg, Manitoba, Canada.

B. McIntosh is with the Department of Physics & Astronomy, University of Manitoba, Winnipeg, Manitoba, Canada.

M.J. Simpson and J. Schellenberg are with Cubresa, Inc., Winnipeg, Manitoba, Canada (e-mail: MSimpson@cubresa.com, JSchellenberg@cubresa.com)

II. Materials and Methods

A. Handheld Gamma Camera Design

A handheld gamma camera, shown in Figure 1, was constructed based on the SensL SPMArray4M silicon photomultiplier (SiPM) detector (SensL Inc., Cork, Ireland) coupled to a CsI:Tl scintillator array. The scintillator array is a 4 × 4 element array, directly coupled to the SiPM using optical grease, with crystal size of 3.3 × 3.3 × 5 mm^3 allowing 1:1 coupling between the scintillator elements and the SiPM pixels in the SPMArray4M. The crystal array uses 3M Enhanced Specular Reflector (ESR) as a reflector between crystals and was obtained from a commercial vendor (Proteus, Inc., Chagrin Falls, OH). A low energy high resolution (LEHR) parallel hole collimator with 1.2 mm flute size, 0.2 mm septa and 23 mm depth is placed in front of the crystal array. The SiPM, scintillator array, collimator and front end electronics are encased in a light tight enclosure with dimensions 114 × 32 × 26 mm^3 made from ABS plastic using 3D printing. The total package weighs approximately 320 g.

B. Readout Electronics

Each SiPM pixel is individually readout using a real-time data acquisition (DAQ) system based on a two channel analog to digital convertor (ADC). In this prototype system, the digitizer is a National Instruments PXI-6132 (National Instruments, Austin, TX), which is a 4 channel, 14 bit ADC with a maximum sample rate of 2.5 MSPS, of which only two channels are used. The digitizer is controlled by a National Instruments PXIe-8101 embedded controller mounted in a PXI chassis which is also used as the data acquisition host computer, running a graphical user interface (GUI) application written in National Instruments LabView. A screen capture of the GUI program is shown in Figure 2. Since the design is for a two channel DAQ system and there are 16 pixels, an 8:1 signal multiplexing approach is used that cycles through the SiPM pixel channel being readout out by the DAQ. In this implementation, a readout rate of 2 MSPS for each DAQ channel was used, thus allowing each SiPM pixel to be sampled every 4 μs. This time is longer than the CsI:Tl scintillator decay constant (~1 μs) so to ensure that each pulse is accurately measured a pulse stretching circuit is

implemented in the front end electronics to stretch the pulse to 20 µs.

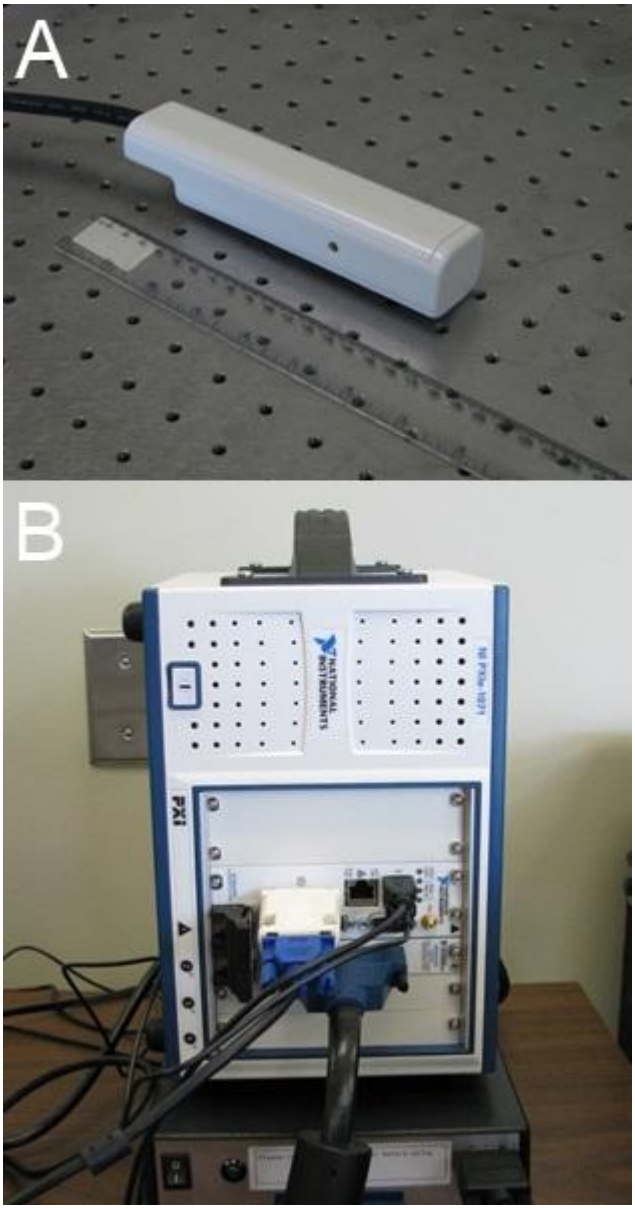

Fig. 1. (A) Photograph of the gamma imaging probe. Note the ruler for scale. (B) Photo of the prototype system electronics.

C. System Characterization

1) Spatial Resolution

The camera was mounted on a two axis translation stage controlled by a PC, which allowed accurate positioning in steps of 2.5 µm. A 0.86 MBq ^{57}Co source (Isotope Products Lab USM02, microPET transmission source, 1 mm active size) was mounted on a stand in front of the face of the detector so that the source was aligned with the center of one of the center rows of scintillator crystals. The detector was stepped in front of the source in steps of 0.5 mm for source-collimator distances of 1, 10, 25, 35 and 50 mm. The 35 mm distance was repeated with an acrylic scattering material between source and camera. Crystal response functions were synthesized for the four crystals in the row at the level of the source as a function of source position. The full width at half maximum (FWHM) spatial resolution was estimated by fitting a Gaussian curve to the crystal response functions. The average and standard deviation of the FWHM for the four crystals in the row is reported.

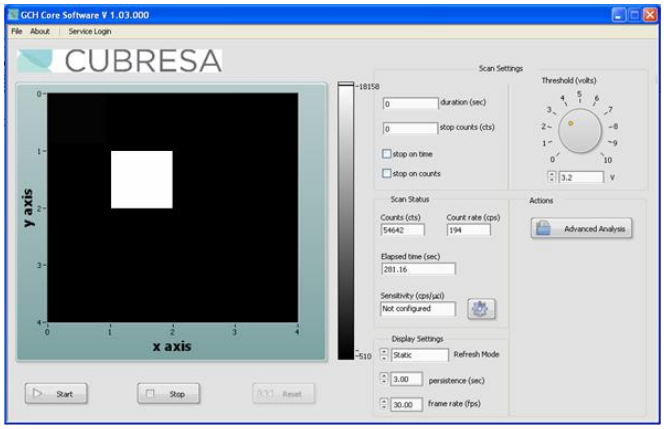

Fig. 2. Screen capture of the GUI application for the prototype system showing the response of the camera to a ^{57}Co point source.

2) Detection Efficiency

The system detection efficiency was calculated by averaging the total count rate for the spatial resolution measurements over the central 8 mm of the detector.

3) Count Rate Performance

The count rate performance of the detector was tested using the method of Geldenhuys et al., normally used for evaluating clinical gamma camera count rate performance [8]. A 350 MBq ^{99m}Tc source was positioned approximately 25 cm from the camera face. The event rate was varied by attenuating the 140 keV gamma-rays with copper sheets. The true event rate was estimated based on the low count rate portion of the curve. For this test the collimator was removed from the camera. The observed count rate is plotted vs. calculated true event rate to examine the system deadtime.

4) Energy Resolution

The FWHM energy resolution at 140 keV was estimated by fitting a Gaussian to the photopeak in the energy spectra data from the count rate test.

III. Results

1) Spatial Resolution

Figure 3 show the crystal response profiles and Gaussian fits to the profiles for source-collimator distances of 1, 10, 35 and 50 mm without scatter and for the 35 mm distance with scatter.

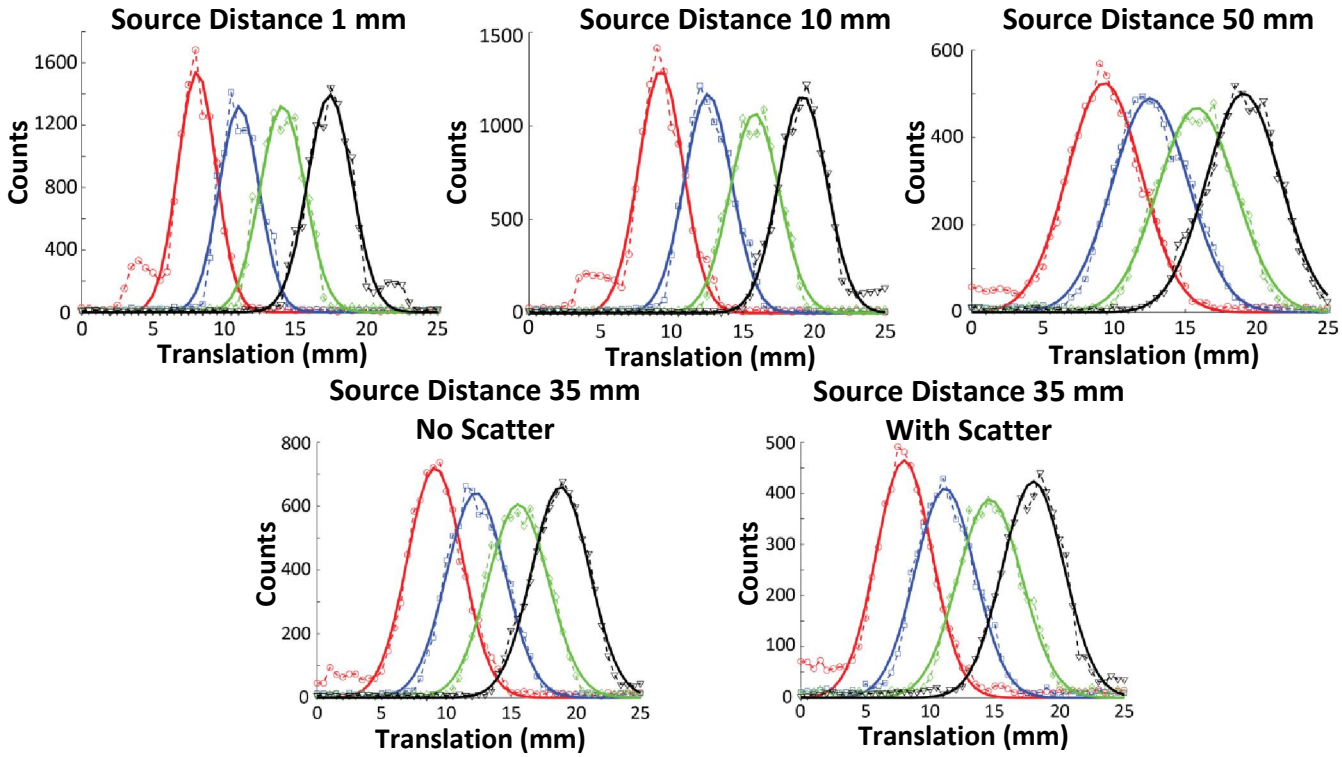

Fig. 3. Crystal response profiles (dashed lines with markers) and Gaussian fits (solid lines) for source-collimator distances of 1, 10, 35 and 50 mm without scatter and 35 mm with scatter. The outer crystal response profiles have a shoulder at the edge, suggesting a potential gap in the camera side shielding. The results suggest that for small source-camera distances the spatial resolution is currently limited by the crystal size used.

As expected, the crystal response profiles are Gaussian in shape, however the outer two crystals have a shoulder on the outer edge, suggesting there may be some penetration of the gamma-rays through the crystal size shielding. Table 1 summarizes the FWHM spatial resolution results for all data collected. As expected, the spatial resolution degrades as the source distance increases due to the parallel hole collimator used. At 1 mm distance, the spatial resolution is 3.46 ± 0.27 mm, dominated by the 3.3 mm size of the scintillator crystal. As the source distance increases to 50 mm, the response of the collimator begins to dominate and the spatial resolution degrades to 6.24 ± 0.13 mm. For the 35 mm distance, introducing a scattering material had minimal impact on the spatial resolution, with the FWHM degrading from 5.28 ± 0.20 mm to 5.50 ± 0.31 mm.

TABLE I. SUMMARY OF SPATIAL RESOLUTION RESULTS

Source-Collimator Distance	FWHM Resolution (mm)
1	3.46 ± 0.27
10	3.92 ± 0.18
25	4.56 ± 0.15
35	5.28 ± 0.20
50	6.24 ± 0.13
35, with scatter	5.50 ± 0.31

2) Detection Efficiency

The average detection efficiency for ^{57}Co for the central 8 mm of the camera FOV with the LEHR collimator in place was 162.9 cps/MBq (0.0163%) for the 1 mm source-collimator distance and 149.7 cps/MBq (0.0150%) for the 50 mm source-collimator distance.

3) Count Rate Performance

Figure 4 shows the plot of observed count rate vs. true event rate for the gamma camera. The response of the camera was linear up to 10^4 cps. Above 10^4 cps the count rate behaved in a super-linear fashion. It is believed that this effect is caused by event pileup leading to a shift in the photopeak position as shown in Figure 5. This is not a concern for routine operation of the camera since the count rates are expected to be in the $10^2 - 10^3$ cps range.

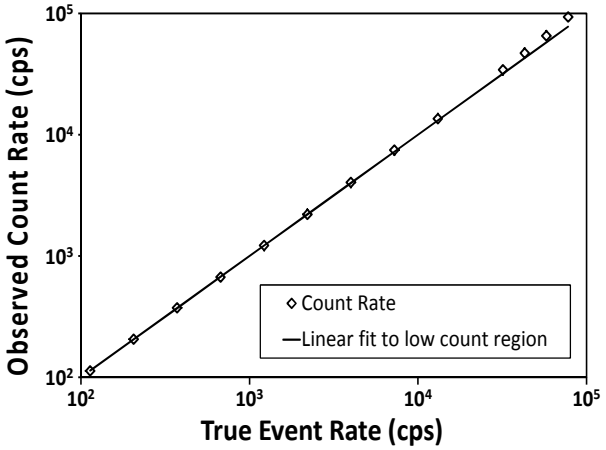

Fig. 4. Observed count rate vs. true event rate for the gamma camera. The true event rate is estimated from the linear fit to the low count region. The camera was linear up to 10^4 cps but above this rate behaved super-linearly due to pileup.

4) Energy Resolution

The FWHM energy resolution at 140 keV was 38.9% at 0.21 kcps and 40.2% at 7.4 kcps. The energy spectra can be seen in Figure 5.

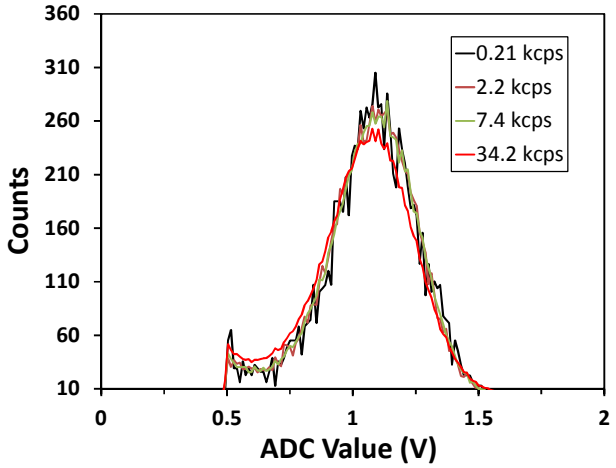

Fig. 5. Plot of the energy spectrum for a ^{99m}Tc source for count rates ranging from 0.2 – 34 kcps. At event rates greater than 10^4 cps there was a shift in the photopeak, likely caused by event pileup.

IV. Discussion and Conclusion

A compact handheld gamma imaging camera was constructed based on the SensL SPMArray4M SiPM array and a CsI:Tl pixelated scintillator array. The camera has a spatial resolution of 3.46 mm at the collimator face and 3.92 mm at a 10 mm distance. The detection efficiency of 162.9 cps/MBq is comparable to other compact imaging cameras that have been developed. Future work will include characterization of the contrast to noise ratio for a variety of lesion detection applications.

References

[1] M. R. S. Keshtgar and P. J. Ell, "Sentinel lymph node detection and imaging," *European Journal of Nuclear Medicine and Molecular Imaging,* vol. 26, p. 11, 1999.

[2] F. Giammarile, N. Alazraki, J. N. Aarsvold, R. A. Audisio, E. Glass, S. F. Grant, *et al.*, "The EANM and SNMMI practice guideline for lymphoscintigraphy and sentinel node localization in breast cancer," *Eur J Nucl Med Mol Imaging,* Oct 2 2013.

[3] P. Olcott, G. Pratx, D. Johnson, E. Mittra, R. Niederkohr, and C. S. Levin, "Clinical evaluation of a novel intraoperative handheld gamma camera for sentinel lymph node biopsy," *Physica Medica,* 2013.

[4] C. Bluemel, A. Schnelzer, A. Okur, A. Ehlerding, S. Paepke, K. Scheidhauer, *et al.*, "Freehand SPECT for image-guided sentinel lymph node biopsy in breast cancer," *Eur J Nucl Med Mol Imaging,* vol. 40, pp. 1656-1661, Oct 2013.

[5] M. Georgiou, G. Loudos, D. Stratos, P. Papadimitroulas, P. Liakou, and P. Georgoulias, "Optimization of a gamma imaging probe for axillary sentinel lymph mapping," *Journal of Instrumentation,* vol. 7, p. P09010, 2012.

[6] K. Kerrou, S. Pitre, C. Coutant, R. Rouzier, P.-Y. Ancel, C. Lebeaux, *et al.*, "The Usefulness of a Preoperative Compact Imager, a Hand-Held Î³-Camera for Breast Cancer Sentinel Node Biopsy: Final Results of a Prospective Double-Blind, Clinical Study," *Journal of nuclear medicine,* vol. 52, pp. 1346-1353, September 1, 2011.

[7] M. Tsuchimochi and K. Hayama, "Intraoperative gamma cameras for radioguided surgery: Technical characteristics, performance parameters, and clinical applications," *Phys Med,* vol. 29, pp. 126-38, Mar 2013.

[8] E. M. Geldenhuys, M. G. Lotter, and P. C. Minnaar, "A New Approach to NEMA Scintillation Camera Count Rate Curve Determination," *J Nucl Med,* vol. 29, pp. 538-541, April 1, 1988.